MULTI-TIME-SCALE DYNAMICS
OF STOCHASTIC ROAD-VEHICLE SYSTEMS

Walter V. Wedig*[1]

[1]KIT, Universität Karlsruhe
wwedig@t-online.de

Keywords: Excitations by roads, multiply iterated integrals, high-order simulations schemes, resonant vehicle speeds, multi-time-scale dynamics, stiff system frequencies, periodograms.

Abstract. *The paper introduces stochastic simulation schemes of arbitrarily high order and covariance equations extended, correspondingly. Both methods are derived by means of multiply iterated integrals and applied to linear road-vehicle systems. Running on roads, vehicles generate vertical vibrations dependent on the vehicle speed. The vibrations become resonant when the ratio of the speed times the road corner frequency approaches the natural frequencies of the vehicle.*

To avoid numerical instabilities in case of high speeds or stiff frequency situations, multi-time-scale dynamics are introduced by scaling the time and noise increments according to the main frequencies of the system. In the stationary case, the co-variances are independent on time so that bigger time steps can be applied to stochastic Euler schemes to estimate the stationary rms-values of scaled dynamic systems provided the applied simulation schemes are stable in mean square.

Best mean-square measurements are utilized to refine the spectral analysis of road profiles and to avoid systematic errors in periodogram evaluations.

1   STOCHASTIC ROAD-VEHICLE SYSTEMS

Measurements show that road-level profiles are random processes. In a first model [1], the road-profile processes are generated from white noise by means of the Itô equation

$$dZ_t = -\bar{v}\Omega Z_t dt + \sigma\sqrt{\bar{v}}\, dW_t, \qquad E(dW_t^2) = dt. \tag{1}$$

Herein, the parameters $\sigma, \Omega > 0$ denote the noise intensity and the road frequency, respectively. Eq. (1) is transformed from the original way domain to time by the way and noise increments $ds = \bar{v}dt$ and $dW_s = \sqrt{\bar{v}}dW_t$ where $\bar{v}$ is the vehicle speed assumed to be positive. In the stationary case, the road-level process Z_t has the following spectrum and mean square:

$$S_z(\omega) = \frac{\sigma^2\bar{v}}{\omega^2 + (\bar{v}\Omega)^2} \;, \qquad \sigma_z^2 = \frac{1}{2\pi}\int_{-\infty}^{+\infty} S_z(\omega)d\omega = \frac{\sigma^2}{2\Omega} \;. \tag{2}$$

According to [2, 3, 4], $\bar{v}\Omega$ is averaged out by integrating the road spectrum over all frequencies $|\omega| < \infty$. This has the consequence that the variance calculated in Eq. (2) is independent on the speed $\bar{v}$ of the vehicle [5].

In figure 1, the road spectrum $S_z(\omega)$ is related to its square mean σ_z^2 and plotted versus the spectral frequency ω in double-logarithm scaling for the three speed parameters $\bar{v}\Omega = 10^0, 10^1, 10^2$. Smooth thick colored lines denote analytical results of the power spectrum calculated by Eq. (2). Overlaid rough black lines represent results of FFT routines applied to numerical solutions of Eq. (1) obtained by means of the stochastic Euler scheme

$$Z_{n+1} = Z_n - \bar{v}\Omega Z_n \Delta t + \sigma\sqrt{\bar{v}}\,\Delta W_n, \qquad \Delta W_n = N_n\sqrt{\Delta t}. \tag{3}$$

The recurrence formula (3) is evaluated for $\Delta t = T/N$ and $n = 0,1,2,\dots$. Hereby, white noise is generated by means of the Wiener increments approximated by normally distributed numbers N_n with zero mean and mean square $E(N_n^2) = 1$. The Fourier series number is chosen to $N = 2^{13}$. Each simulation possesses the time length $T = 10\ s$. They are averaged together with $M = 10^4$ samples. In the high frequency domain, the spectral density is limited by the Fourier series number. The lower frequencies are bounded by finite simulation lengths.
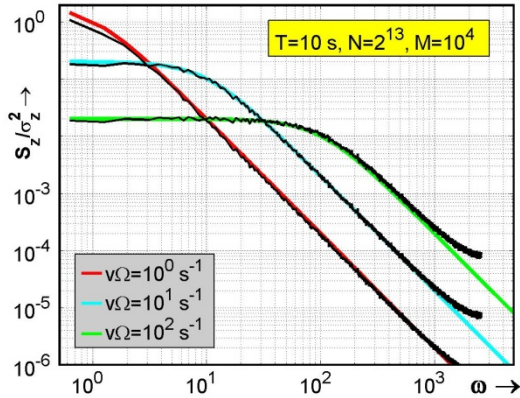

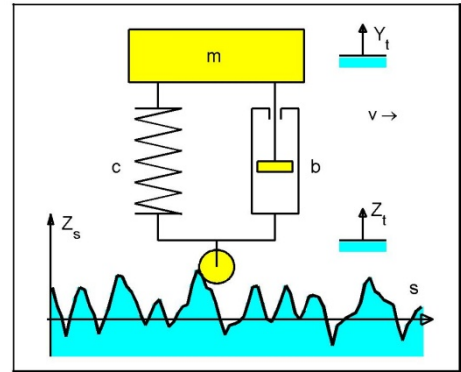| |
| --- |
| Figure 1: Spectra of road profiles in double-logarithmic scaling |

Figure 2: Scheme of road-vehicle systems with one DoF quarter car model

As shown in figure 2, the simulated road process is applied as base excitation of a quarter car model with one degree of freedom described by the equation of motion

$$\ddot{Y}_t + 2D\omega_1(\dot{Y}_t - \dot{Z}_t) + \omega_1^2(Y_t - Z_t) = 0, \qquad \dot{Y}_t = \omega_1 U_t. \tag{4}$$

Herein, Y_t and U_t denote the absolute vertical vehicle displacement and its time derivative, respectively. The vehicle possesses the natural squared frequency $\omega_1^2 = c/m$ and the viscous damping $2D\omega_1 = b/m$. The introduction of $dY_t = \omega_1 U_t dt$ and Eq. (1) into Eq. (4) leads to

$$dU_t = -\omega_1(Y_t - Z_t)dt - 2D(\omega_1 U_t + \bar{v}\Omega Z_t)dt + 2D\sigma\sqrt{\bar{v}}dW_t.$$

Therewith, the road-vehicle system is described by the three-dimensional vector equation

$$dV_t = AV_t dt + g dW_t, \qquad V_t = (Y_t, U_t, Z_t)' . \tag{5}$$

It has the three-dimensional vectors g, V_t and the 3x3 system matrix, as follows:

$$g = \begin{bmatrix} 0 \\ 2D \\ 1 \end{bmatrix} \sigma\sqrt{\bar{v}}, \qquad A = \begin{bmatrix} 0 & 1 & 0 \\ -\omega_1 & -2D\omega_1 & \omega_1 - 2D\bar{v}\Omega \\ 0 & 0 & -\bar{v}\Omega \end{bmatrix}.$$

Applying the root-mean-square $\sigma_z = \sigma/\sqrt{2\Omega}$, the state processes of excitation and response are appropriately scaled by $(Y_t, U_t, Z_t) = \sigma_z(\bar{Y}_t, \bar{U}_t, \bar{Z}_t)$ such that $E(\bar{Z}_t^2) = 1$.

2 HIGHER ORDER SIMULATION SCHEMES

To derive higher order simulation schemes, the increment equation (5) is rewritten into the form of the equivalent integral equation (see also Ref. [6,7,8])

$$V_{t+\Delta t}^{(n+1)} = V_t + A\int_t^{t+\Delta t} V_\tau^{(n)} d\tau + g \int_t^{t+\Delta t} dW_\tau , \qquad n = 0,1,2,\dots \quad . \tag{6}$$

Herein, V_t is the initial vector at time $\Delta t = 0$. The integral Eq. (6) is iteratively solved for $n = 0,1,2,\dots$ starting with the zero solution $V_\tau^{(0)} = V_t$. The iteration procedure leads to multiply iterated integrals which are evaluated [9] in the mean square sense, as follows:

$$V_{t+\Delta t} = V_t + BV_t\Delta t + h\Delta W_t, \qquad \Delta W_t = \sqrt{\Delta t}N_n. \tag{7}$$

This result represents an explicit simulation scheme derived in [9]. It is determined by

$$B = \left[I + \frac{1}{2!}(A\Delta t) + \dots + \frac{1}{(n+1)!}(A\Delta t)^n + \cdots\right]A, \tag{8}$$

$$h = \left[I + \frac{1}{1!\sqrt{3}}(A\Delta t) + \cdots + \frac{1}{n!\sqrt{2n+1}}(A\Delta t)^n + \cdots\right]g. \tag{9}$$

Herein, I is the $m x m$ unit matrix, B is a $m x m$ drift matrix and h a m-dimensional diffusion vector. The m-dimensional vector equation (7) is multiplied by its transposed form in order to derive the following extended covariance equation [10] for the mxm co-variance matrix P.

$$BP + PB' + BPB'\Delta t + hh' = 0, \qquad P = E(V_t V_t'). \tag{10}$$

Note that the applied method of multiply iterated integrals leads to the drift matrix B that coincides in the form $I + B\Delta t$ with the exponential matrix $\exp(A\Delta t)$ of linear homogeneous systems. However, the diffusion vector noted in Eq. (9) is new with terms scaled by the square root of $2n + 1$. This is a consequence of the mean square analysis applied in order to calculate the multiply iterated integrals, explicitly.

To show some more details of derivation, consider e.g. the iterated double integral $I_{1,t}$ which is easily once integrated with respect to noise and also with respect to time by interchanging the sequence of both integrations. Both integrations yield

$$I_1,t = \int_t^{t+\Delta t}\int_t^\tau dW_{\tau_1} d\tau = \int_t^{t+\Delta t}(W_\tau - W_t)d\tau, \tag{11}$$

$$I_1,t = \int_t^{t+\Delta t}(t + \Delta t - \tau_1)dW_{\tau_1} \cong \frac{1}{\sqrt{3}}\Delta W_t\Delta t. \tag{12}$$

Obviously, the noise-time integral (11) can also be derived from the time-noise integral (12) by means of the rule of partial integration. Both integrals are normally distributed. They are stationary with zero mean and mean square independent on time. For decreasing time and noise increments, the double integral is proportional to the integration area $\Delta W_t \Delta t$ with the proportional factor $1/\sqrt{3}$ calculated in mean square sense, as follows:

$$E(I_{1,t}^2) = \iint_t^{t+\Delta t} E\big[(W_{\tau_1} - W_t)(W_{\tau_2} - W_t)\big] d\tau_1 d\tau_2 = \tfrac{1}{3}\Delta t^3, \qquad (13)$$

$$E(I_{1,t}^2) = \iint_t^{t+\Delta t} (t + \Delta t - \tau_1)(t + \Delta t - \tau_2) E(dW_{\tau_1} dW_{\tau_2}) = \tfrac{1}{3}\Delta t^3. \qquad (14)$$

The result in Eq. (13) is derived applying $E(W_{t_1} W_{t_2}) = \min(t_1, t_2)$. The second expectation in Eq. (14) is even simpler and directly evaluated by means of $E(dW_t dW_s) = 0$ for $t \neq s$ and $E(dW_t^2) = dt$. The results of Eqs. (13, 14) coincide with $E[(\Delta W_t \Delta t/\sqrt{3})^2] = \Delta t^3/3$, q.e.d.

The integration scheme derived in Eq. (7) is applied to the quarter car model shown in Fig. 3. It has two degrees of freedom described by the two equations of motion

$$\ddot{Y}_t + 2D\omega_1 \dot{R}_t + \omega_1^2 R_t = 0, \qquad R_t = Y_t - Y_t,$$

$$\ddot{X}_t - 2D\omega_1 \mu \dot{R}_t - \omega_1^2 \mu R_t + \omega_2^2 (X_t - Z_t) = 0.$$

Herein, Y_t and X_t denote the absolute vibration coordinates of the vehicle and wheel masses M and m, respectively. The process R_t determines the relative motion of both masses. The equations of motion possess the reference frequencies $\omega_1^2 = c/M$ and $\omega_2^2 = k/m$. The energy dissipation of the system is modeled by the viscous damper D, and the mass ratio is denoted by $\mu = M/m$. Figure 4 shows the related rms-values of the stationary vehicle and wheel vibrations for the frequencies $\omega_1 = 1$ and $\omega_2 = 10$, the scan rate $\Delta t = 0.025$, the mass ratio $\mu = 4$ and the damping values $D = .03, .05$ and 0.1. All rms-results are calculated by means of the covariance equation (10) and subsequently simulated via the forth $(n = 3)$ order integration scheme (7) applied for the step size $\Delta t = .025$ and $M = 10^6$ samples.
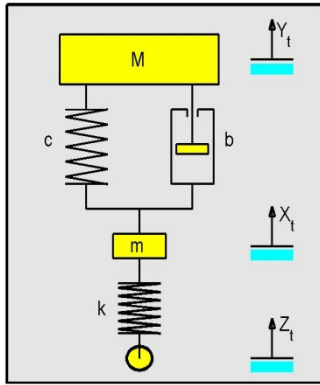

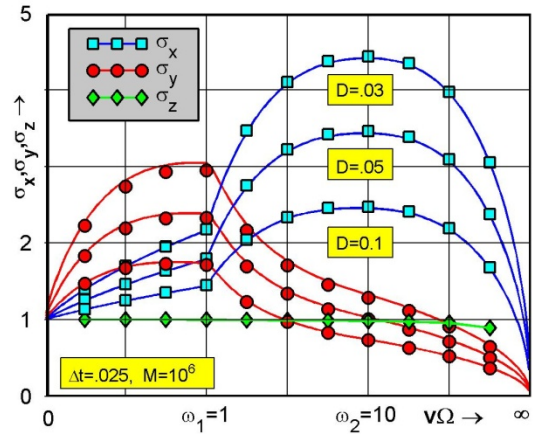Figure 3: Quarter car model [11]
with two degrees of freedom

Figure 4: Simulated rms-values applying
a forth order scheme by Eq. (7)

The results obtained are plotted versus the speed parameter $\bar{v}\Omega$ and the design parameter λ with the following linear scaling in the first and middle range and a hyperbolic scaling in the last third range as already applied to the linear harmonic oscillator in [12]. Obviously, there are two resonant speeds: a first one near $\omega_1 = 1$ where the red rms-values of the vehicle

vibrations become resonant, and a second one near $\omega_2 = 10$ where the blue rms-values of the wheel vibrations are maximal. For vanishing speed, there are no magnifications; i.e. vehicle and wheel follow the road level, identically. For infinitely increasing speed, all system responses are vanishing. Green diamonds stand for measured rms of the excitation.

$$I:\ 0 \leq \lambda \leq 1 \qquad\qquad (\bar{v}\Omega)_I = \lambda\omega_1,$$
$$II:\ 1 \leq \lambda \leq 2 \qquad\qquad (\bar{v}\Omega)_{II} = (2 - \lambda)\omega_1 + (\lambda-1)\omega_2,$$
$$III:\ 2 \leq \lambda \leq 3 \qquad\qquad (\bar{v}\Omega)_{III} = \omega_2/(3 - \lambda).$$

The covariance analysis presented in figure 4 shows the typical integration difficulties of stiff dynamical systems. For low frequency speeds $\bar{v}\Omega \ll 1$, first order Euler schemes are sufficient to predict the stationary rms-values of the road-vehicle system. For increasing velocities, the influence of the stiff frequency ratio realistically chosen [11] to $\omega_2/\omega_1 = 10$, becomes stronger and has to be balanced by higher order integration schemes. For infinitely increasing speed frequencies $\bar{v}\Omega \to \infty$, higher order simulation schemes lead to growing errors, as well and become unstable, finally.

3 REFINED SPECTRAL ANALYSIS OF ROAD PROFILES

As already mentioned, one-dimensional profiles of road levels Z_s are measured in the way domain. Accordingly, they are modelled by the way differential equation

$$dZ_s = -\Omega Z_s ds + \sigma dW_s, \qquad E(dW_s^2) = ds. \tag{15}$$

Herein, ds is the increment of the length coordinate s, dW_s is the associated Wiener increment of intensity $\sigma \geq 0$ and $\Omega > 0$ is a road corner frequency with dimension $1/m$. Applying the Fourier transform to Eq. (15), the spectral density distribution of Z_s is calculated to

$$S_z(w) = \frac{\sigma^2}{\Omega^2+w^2}, \qquad\qquad \sigma_z^2 = \frac{1}{\pi}\int_0^\infty S_z(w)dw = \frac{\sigma^2}{2\Omega}. \tag{16}$$

The integration with respect to the way frequencies $|w| < \infty$ leads to the same variance σ_z^2 of the one-dimensional road level profile, as already noted in Eq. (2).

To extend this analysis to higher order road models, consider e.g. the third order system

$$X_s''' + 2\alpha\Omega X_s'' + 2\beta\Omega^2 X_s' + \Omega^3 X_s = \sigma W_s', \qquad \alpha, \beta = 1. \tag{17}$$

Herein, dashes denote derivatives with respect to the length coordinate s. For the parameters $\alpha = \beta = 1$, the extended road model possesses the following spectrum and variance:

$$S_x(w) = \frac{\sigma^2}{\Omega^6+w^6}, \qquad\qquad \sigma_x^2 = \frac{1}{\pi}\int_0^\infty S_x(w)dw = \frac{\sigma^2}{3\Omega^5}. \tag{18}$$

Introducing the first and second derivative by $X_s' = \Omega U_s$ and $U_s' = \Omega V_s$, respectively, the road model equation (17) is rewritten into the first order increment form

$$dX_s = \Omega U_s ds, \qquad dU_s = \Omega V_s ds, \qquad \sigma_u^2 = \sigma^2/(6\Omega^5), \tag{19}$$

$$dV_s = -\Omega(2V_s + 2U_s + X_s)ds + \sigma dW_s/\Omega^2, \qquad \sigma_v^2 = \sigma^2/(3\Omega^5). \tag{20}$$

These increment equations are numerically investigated using a sixth order integration scheme.

The application of the Fourier transform to the stochastic road profile X_s yields the complex spectrum $X_L(w)$. The multiplication by the conjugate version $X_L^*(w)$ gives

$$\bar{S}_x(w) = \lim_{L\to\infty}\frac{1}{L}X_L(w)X_L^*(w), \qquad X_L(w) = \int_0^L X_s \exp(iws)\, ds.$$

This form of a power spectrum is called periodogram because the expected value $E[\bar{S}_x(w)]$ coincides with the mean value of the power spectrum but it is not possible to proof its square-mean convergence. To overcome this difficulty, the road process is cut e.g. after the length $L = 600 \, m$. This implies that the discrete Fourier transformation can be applied by

$$X_L(w_n) = u_n \Delta s, \qquad u_n = \sum_{k=0}^{N-1} X_k \exp\left(-ink\frac{2\pi}{N}\right).$$

Herein, X_k are N discrete values of the process X_s scanned with the step size $\Delta s = L/N$ for e.g. $N = 2^{13}$ measurements. Accordingly, the spectral values u_n are taken at the frequencies $w_n = n w_L$ where n= $1,2,\dots N$ and w_L is the base frequency of the Fourier series given by $w_L = 2\pi/L$. When further measurements $m = 1,2,\dots M$ of the same length are available, the FFT routine is repeated to each measurement and averaged with all other FFT results.

$$\bar{S}_x(w_n) = \frac{\Delta s}{NM} \sum_{m=1}^{M} u_{nm}(w_n)u_{nm}^*(w_n), \qquad \text{for all } n = 01,2,\dots N/2. \qquad (21)$$
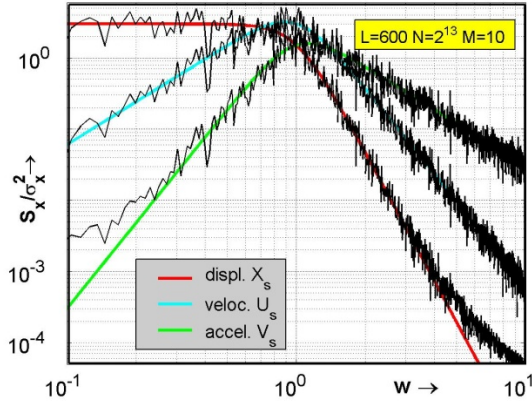

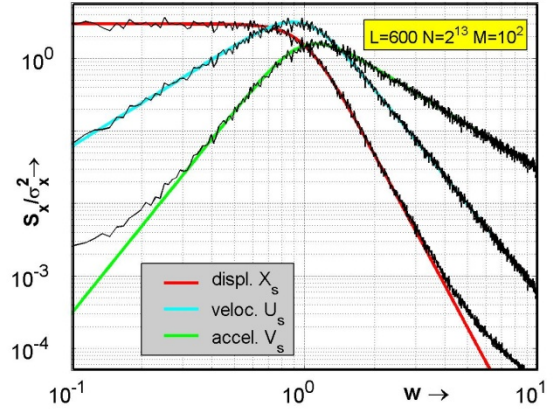Figure 5: Numerical FFT-evaluations applied for $M = 10$ simulation samples.

Figure 6: Convergence of FFT routines overlaid by analytic spectra for $\Omega = 1$.

Finally, the square mean value $E(X_s^2)$ of all measurements is calculated, additionally and separately to introduce a correction c_x into the spectral result, as follows:

$$\hat{S}_x(w_n) = c_x \sum_{m=1}^{M} u_{nm}(w_n)u_{nm}^*(w_n), \qquad (22)$$

$$E(X_s^2) = \frac{1}{\pi} \int_0^{+\infty} S_x(w)dw = \frac{1}{\pi} \sum_{n=0}^{N/2} \hat{S}_x(w_n)\Delta w_L. \qquad (23)$$

The insertion of Eq. (22) into (23) leads to

$$c_x = \frac{\pi}{\Delta w_L} E(X_s^2)/[\sum_{n=0}^{N/2} \sum_{m=1}^{M} u_{nm}(w_n)u_{nm}^*(w_n)]. \qquad (24)$$

By means of the correction factor c_x, the spectral density (22) is statistically consistent.

M	10^1	10^2	10^3
S_x	26.005	8.0471	4.2740
S_u	26.549	8.2014	4.4054
S_v	26.524	9.1929	5.9109

Table 1: Relative error of S_x, S_u, S_v for M=$10^1, 10^2, 10^3$

Corresponding numerical results are represented in figure 5 and 6 for samples chosen by $M = 10$ and 100. Smooth thick colored lines are analytical results of the displacement, veloc-

ity and acceleration spectra. Overlaid rough black lines represent averaged results of FFT routines corrected by the mean-square $E(X_s^2)$, measured additionally. As shown in table 1, the relative error of the FFT evaluations becomes smaller with growing sample number M.

4   MULTI-SCALED COVARIANCE ANALYSIS

In the following, the mean square estimation previously applied is extended with respect to convergence and stability. To introduce these extensions, consider the first order system (1) of the base excitation Z_t and the Euler scheme (3), normalized by $\bar{Z}_t = Z_t/\sigma_z$:

$$\bar{Z}_{t+\Delta t} = \bar{Z}_t - \bar{v}\Omega\bar{Z}_t\Delta t + \sqrt{2\bar{v}\Omega}\,\Delta W_t, \qquad \rho = 1 - \bar{v}\Omega\Delta t. \tag{25}$$

Squaring this simulation scheme and taking the expectation on both sides, yields

$$E(\bar{Z}_{t+\Delta t}^2) = [1 - 2\bar{v}\Omega\Delta t + (\bar{v}\Omega\Delta t)^2]E(\bar{Z}_t^2) + 2\bar{v}\Omega\Delta t\,. \tag{26}$$

In the stationary case, the square means are independent on time that leads to

$$E(\bar{Z}_t^2) = \frac{1}{1-\bar{v}\Omega\Delta t/2}\,, \qquad \text{stable for} \qquad 0 \le \Delta t \le 2/\bar{v}\Omega\,. $$

Accordingly, the mean square estimation possesses the correction $1/(1 - \bar{v}\Omega\Delta t/2)$ of the true value $E(\bar{Z}_t^2) = 1$ and therewith relative errors which are increasing with growing time steps of simulation. In the limiting case, when Δt exceeds $2/\bar{v}\Omega$ the estimated mean square becomes infinite and then negative, i.e. it is no more physically existent. Obviously, this existence condition coincides with the stability condition $|\rho| \le 1$ that the absolute value of the characteristic multiplier ρ is less than one. Figure 8 shows the typical behaviour of the related mean square $E(\bar{Z}_t^2)$ for a fixed small step size $\Delta t = .01$ and infinitely increasing vehicle speed. The rms-values calculated by means of the covariance equation (10) are marked by interrupted magenta lines for the first order approximation, respectively by solid lines for the corresponding second order result. The application of Itô's formula [13] to Eq. (1) leads to

$$d(\bar{Z}_t^2) = 2\bar{v}\Omega(1 - \bar{Z}_t^2)dt + 2\sqrt{2\bar{v}\Omega}\,\bar{Z}_t dW_t. \tag{27}$$

$$\bar{Z}_{t+\Delta t}^2 = \bar{Z}_t^2 + 2\bar{v}\Omega(1 - \bar{Z}_t^2)\Delta t + 2\sqrt{2\bar{v}\Omega}\,\bar{Z}_t \Delta W_t. \tag{28}$$

The Eq. (28) is an integration scheme to be applied for all time steps $n\Delta t$. With the stationarity condition $E(\bar{Z}_{t+\Delta t}^2) = E(\bar{Z}_t^2)$, the simulation scheme (28) possesses the expected solution

$$E(\bar{Z}_t^2) = 1, \qquad \text{stable for} \qquad 0 \le \Delta t \le 1/(\bar{v}\Omega). $$

In comparison with the linear Eq. (25), the bi-linear simulation (28) works without systematic errors. Hence, it is independent on the scan rate Δt and asymptotically stable in mean square when the time step size selected is smaller than $1/(\bar{v}\Omega)$.

The advantage of the bi-linear mean square estimations that they are independent on step sizes is utilized to introduce a multi-time scaling into the dynamics of road-vehicle systems. For this purpose, a different time scaling of the squared process $\bar{Z}_t^2$ and the two bi-linear processes $\bar{X}_t\bar{Z}_t$ and $\bar{U}_t\bar{Z}_t$ has to be simulated, simultaneously. According to [13], the application of Itô's calculus to the bi-linear processes leads to the increment equations

$$d(\bar{Z}_t\bar{X}_t) = -\bar{v}\Omega\bar{Z}_t\bar{X}_t dt + \omega_1\bar{Z}_t\bar{U}_t dt + \sqrt{2\bar{v}\Omega}\,\bar{X}_t dW_t, \tag{29}$$

$$d(\bar{Z}_t\bar{U}_t) = -\omega_1\bar{Z}_t\bar{X}_t dt - (2D\omega_1 + \bar{v}\Omega)\bar{Z}_t\bar{U}_t dt + 4D\bar{v}\Omega dt$$

$$+ (\omega_1 - 2D\bar{v}\Omega)\bar{Z}_t^2 dt + \sqrt{2\bar{v}\Omega}(\bar{U}_t + 2D\bar{Z}_t)dW_t. \tag{30}$$

To obtain better simulation schemes, we introduce the time und noise increments $\omega_1 dt = d\tau$ and $\sqrt{\omega_1} dW_t = dW_\tau$ into the co-variance equations (29) and (30) as well as a second scaling by means of the increments $\bar{v}\Omega dt = d\sigma$ und $\sqrt{\bar{v}\Omega}\, dW_t = dW_\sigma$ into the excitation equation (25). Therewith, the Itô equations (27), (29) and (30) lead to the following Euler schemes:

$$\bar{Z}_{\sigma+\Delta\sigma}^2 = \bar{Z}_\sigma^2 - 2\bar{Z}_\sigma^2\Delta\sigma + 2\Delta\sigma + 2\sqrt{2}\,\bar{Z}_\sigma\Delta W_\sigma, \tag{31}$$

$$(\bar{Z}_\tau\bar{X}_\tau)_{\tau+\Delta\tau} = \bar{Z}_\tau\bar{X}_\tau - (v\bar{Z}_\tau\bar{X}_\tau - \bar{Z}_\tau\bar{U}_\tau)\Delta\tau + \sqrt{2v}\bar{X}_\tau\Delta W_\tau, \tag{32}$$

$$(\bar{Z}_\tau\bar{U}_\tau)_{\tau+\Delta\tau} = \bar{Z}_\tau\bar{U}_\tau - [\bar{Z}_\tau\bar{X}_\tau + (2D+v)\bar{Z}_\tau\bar{U}_\tau - 4Dv]\Delta\tau$$
$$+ (2Dv-1)\bar{Z}_\tau^2\Delta\tau + \sqrt{2v}(\bar{U}_\tau + 2D\bar{Z}_\tau)\Delta W_\tau. \tag{33}$$

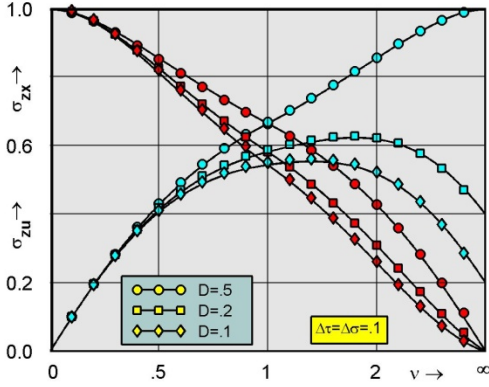Herein, the parameter v stands for the speed frequency ratio $v = \bar{v}\Omega/\omega_1$.

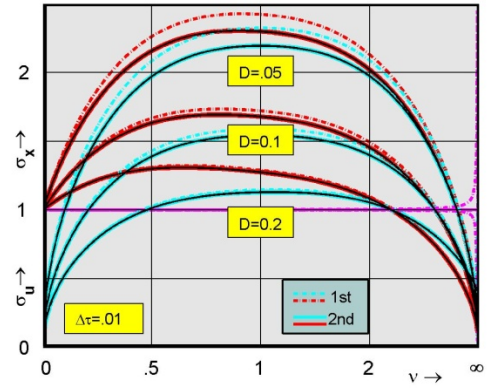Figure 7: Simulated co-variances of response and excitation processes

Figure 8: 1st and 2nd order rms overlaid by strong results marked by thin black lines.

Note that the simulation equations (31), (32) and (33) can be applied for arbitrary and different step sizes $\Delta\tau \neq \Delta\sigma$ provided that the simulation routines are stable. In the stationary case, the expected values are given by $E(\bar{Z}_\sigma\Delta W_\sigma) = 0$ and $E(\bar{Z}_{\sigma+\Delta\sigma}^2) = E(\bar{Z}_\sigma^2)$. Therewith, Eq. (31) leads to the stationary mean square result $E(\bar{Z}_\sigma^2) = 1$ which is independent on the scan rate $\Delta\sigma$ and frequency ratio v. In the stationary case, the two further simulation equations (32) and (33) lead to the displacement and velocity co-variances

$$\sigma_{zx}^2 = E(\bar{Z}_\tau\bar{X}_\tau) = \frac{1+2Dv}{1+2Dv+v^2}, \qquad \sigma_{zu}^2 = E(\bar{Z}_\tau\bar{U}_\tau) = \frac{(1+2Dv)v}{1+2Dv+v^2}. \tag{34}$$

They are also independent on the applied scan rate $\Delta\tau$ and strong without any systematic error. In the bilinear simulation equations (31), (32) and (33), the perturbations by noise appear in multiplicative form multiplied by the linear processes $\bar{Z}_\sigma, \bar{Z}_\tau, \bar{X}_\tau, \bar{U}_\tau$. Consequently, the linear processes have to be simulated, simultaneously. This is performed by the Euler scheme

$$\bar{Z}_{\sigma+\Delta\sigma} = \bar{Z}_\sigma - \bar{Z}_\sigma\Delta\sigma + \sqrt{2}\,\Delta W_\sigma, \qquad \bar{X}_{\tau+\Delta\tau} = \bar{X}_\tau + \bar{U}_\tau\Delta\tau,$$

$$\bar{U}_{\tau+\Delta\tau} = \bar{U}_\tau - [\bar{X}_\tau - \bar{Z}_\tau + 2D(\bar{U}_\tau + v\bar{Z}_\tau)]\Delta\tau + 2D\sqrt{2v}\,\Delta W_\tau.$$

However, because of $E(\bar{X}_\tau\Delta W_\tau) = 0$ and $E(\bar{U}_\tau\Delta W_\tau) = 0$, the results of the linear equations don't influence the stationary solutions (34) provided the linear simulation is stable.

In figure 7, simulation results of the bi-linear equations (32, 33) are calculated for the damping values $D = .5, .2, .1$ marked by red and cyan circles, squares and diamonds, respectively. They are compared with the black lines of the strong values $E(\bar{Z}_\tau\bar{X}_\tau)$ and $E(\bar{Z}_\tau\bar{U}_\tau)$.

The step size selected was $\Delta\tau = 0.1$ and $\Delta\sigma = 0.1$ both applied for 10^6 sample points. The co-variances are plotted versus the speed ratio $v = \bar{v}\Omega/\omega_1$ applying a linear scaling in the first half range and a hyperbolic scaling [12] in the last half range.

$$I: 0 \leq \lambda \leq 1 \qquad\qquad v = \lambda,$$
$$II: 1 \leq \lambda \leq 2 \qquad\qquad v = 1/(2 - \lambda).$$

According to Eqs. (34), the displacement co-variance starts with one for vanishing speeds and ends with zero when speed tends to infinity. Inversely, the velocity co-variances start with zero and end with the finite value $2D$ for high vehicle speeds. Note that the co-variance analysis is performed by two time-scales of the road-vehicle system. The simulation works without systematic errors provided that the simulation is stable. To investigate the stability in mean square, the bi-linear simulation equations (32) and (33) are checked by

$$\begin{vmatrix} \rho - 1 + v\Delta\tau & -v\Delta\tau \\ v\Delta\tau & \rho - 1 + (2D + v)\Delta\tau \end{vmatrix} = 0.$$

This determinant gives the multiplier ρ and leads to the mean square stability condition

$$2(D + v) \geq (1 + 2Dv + v^2)\Delta\tau, \quad \text{for} \quad D \leq 1.$$

In the limiting case of infinitely increasing speed, this condition gives the critical step size by $\Delta\tau \leq 2/v$. Inversely, when the vehicle slows down, the step size of stable simulations is bounded by $\Delta\tau \leq 2D$. Once, when the co-variances are calculated the remaining quadratic processes are determined by the stochastic Euler schemes

$$\bar{X}^2_{t+\Delta t} = \bar{X}^2_t + 2\omega_1 \bar{X}_t \bar{U}_t \Delta t, \qquad\qquad\qquad \text{Abbr.:} \quad v_D = 1 - 2Dv,$$

$$\bar{U}^2_{t+\Delta t} = \bar{U}^2_t + 2\omega_1(4D^2 v - 2D\bar{U}^2_t - \bar{X}_t\bar{U}_t + v_D\bar{Z}_t\bar{U}_t)\Delta t + 4D\sqrt{2v\omega_1}\,\bar{U}_t\Delta W_t,$$

$$(\bar{X}\bar{U})_{t+\Delta t} = \bar{X}_t\bar{U}_t + \omega_1(\bar{U}^2_t - \bar{X}^2_t - 2D\bar{X}_t\bar{U}_t + v_D\bar{Z}_t\bar{X}_t)\Delta t + 2D\sqrt{2v\omega_1}\,\bar{X}_t\Delta W_t.$$

They are applicable using a third time scale given e.g. by $D\omega_1\Delta t = \Delta\xi$ and $\sqrt{D\omega_1}\Delta W_t = \Delta W_\xi$. In the stationary case, these equations possess the expected solutions $E(\bar{X}_t\bar{U}_t) = 0$ and

$$E(\bar{U}^2_t) = \frac{1}{2D}[4D^2 v + v_D E(\bar{Z}_t\bar{U}_t)] = \frac{v}{2D}\frac{1 + 4D^2(1 + 2Dv)}{1 + 2Dv + v^2},$$

$$E(\bar{X}^2_t) = E(\bar{U}^2_t) + v_D E(\bar{Z}_t\bar{X}_t) = \frac{1}{2D}\frac{v + 2D(1 + 2Dv)}{1 + 2Dv + v^2}.$$

In figure 8, the correct results of the bi-linear Euler schemes are marked by thinner black lines and plotted versus the frequency speed $v = \bar{v}\Omega/\omega_1$. Overlaid colored interrupted and solid lines denote corresponding first, respectively second order approximations, calculated by the extended covariance equation (10) for the scan rate $\Delta\tau = .01$ and the damping $D = .05, .1, .2$. The comparison of both results shows that the simulation of linear processes always leads to systematic errors which are reducible by means of smaller scan rates and higher order simulation schemes. The bi-linear process simulation, however, works without systematic errors.

5. CONCLUSIONS

The paper introduces high order simulation schemes and correspondingly extended covariance equations. Both are derived by multiply iterated integrals and applied to road-vehicle systems. Running on roads, the car generates vertical vibrations. They depend on the car velocity and become resonant when the vehicle speed times the road frequency approaches the natural circle frequencies of the vehicle.

To avoid simulation instabilities in case of high speeds or stiff frequency situations, multi-time scales are introduced by time and noise increments chosen according to the main frequencies of the system. In the stationary case, the co-variances are independent on time so that big time steps can be applied in stochastic Euler schemes to simulate and estimate the stationary rms-values of the scaled dynamic system without any systematic error.

Optimal mean-square measurements are utilized to refinements of the spectral analysis in order to obtain statistically consistent periodograms evaluations of road profiles. This technique avoids systematic errors by maintaining the one-dimensional characteristics. In a second step, the evaluations of the stationary signals are extended to two-dimensional characteristics; i.e. correlations and spectra are only statistically correct when mean values and square means of the roads profiles are maintained.

REFERENCES

[1] W. Wedig, Dynamics of Cars Driving on Stochastic Roads. P.D. Spanos & G. Deodatis eds. *Proc. of Computational Stochastic Mechanics,* Millpress, Rotterdam, 647-54, 2003.

[2] K. Sobczyk, D.B. MacVean & J.D. Robson, Response to Profile-Imposed Excitation with Randomly Varying Transversal Velocity. *J. Sound and Vibration*, 52, 1, 37-49, 1977.

[3] B.R. Davis & A.G. Thompson, Power Spectral Densty of Road Profiles. *Vehicle System Dynamics*, 35, 6,409-415, 2001.

[4] C.J. Doods CJ & J.D. Robson, The Description of Road Surface Roughness. *Journal Sound and Vibration*, 31, 2, 175-183, 1973.

[5] K. Popp & W.O. Schiehlen, *Fahrdynamik.* Teubner-Verlag, Stuttgart, 1993.

[6] G.N. Milshtein, Approximate Integration of Stochastic Differential Equations. *Journal Theory Prob. Appl.,* 30,750-766, 1985.

[7] P.E. Kloeden & E. Platen, *Numerical Solution of Stochastic Differential Equations.* Springer-Verlag, 1992.

[8] D. Talay, Simulation and Numerical Analysis of Stochastic Differential Systems: A Review. *Probabilistic Methods in Applied Physics.* P. Krée, W. Wedig eds. Lecture Notes in Physics 451. Springer, 54-96, 1995.

[9] W.V.Wedig, Resonances of Road-Vehicle Systems with Nonlinear Wheel Suspensions. IUTAM-Symposium on *Dynamics Modelling and Interaction Control in Real and Virtual Environments. G.* Stépán, L.L. Kovács, A. Tóth eds. Springer, 83-90, 2010.

[10] W.V. Wedig, Simulation of Road-Vehicle Systems. *Prob. Eng. Mech.,* 27,1,82-87,2012.

[11] D. Ammon, *Modellbildung und Systementwicklung in der Fahrzeugdynamik.* Teubner-Verlag, Stuttgart,1997.

[12] K. Klotter, *Technische Schwingungslehre.*Bd.1, 3. Aufl. Springer, 1978.

[13] L. Arnold, *Stochastic Differential Equations.* New York, Wiley, 1974.